

FAULT DIAGNOSIS FOR SENSOR AND ACTUATOR OF HEXACOPTER UAV USING DUAL EXTENDED KALMAN FILTER

Yeji Kim¹, Taegyun Kim¹ & Seungkeun Kim¹

¹Department of Aerospace Engineering, Chungnam National University, Daejeon, Republic of Korea

Abstract

This paper performs the fault diagnosis for the hexacopter attitude control system using a dual extended Kalman filter (EKF). Fault detection and diagnosis (FDD) is conducted by using the analytical redundancy of angular rates. Two EKFs are designed for dynamics and kinematics of angular rates, respectively. Fault detection of the IMU sensor and actuator is conducted using these two EKFs. The performance of the fault detection algorithm is verified through numerical simulation. The simulation results demonstrate that the proposed fault detection algorithm can not only detect the complete fault of the IMU sensor and actuator but also detect the partial fault of the IMU sensor.

Keywords: Fault detection and diagnosis, Extended Kalman filter, IMU sensor, Actuator, Hexacopter UAV

1. Introduction

Unmanned aerial vehicles (UAVs), especially multirotor UAVs, have been developed in various ways and are widely used. Since UAVs can carry several types of equipment, it is being developed not only for military purpose but also for civilian applications such as rescue and media. Recently, the development of delivery drones operated in urban and suburban areas has been in the spotlight [1, 2]. As the operating range of UAVs expands to urban areas, a very high level of safety and reliability is required for the aircraft. Although most modern vehicles are equipped with fault detection and isolation systems, accidents due to sensor and actuator failures still occur [3]. Therefore, research on fault diagnosis and response techniques is significantly important and essential.

Fault detection and isolation (FDI) methods are classified into three methods: hardware redundancy, analytical redundancy, and signal processing [4]. Among them, hardware redundancy, which uses multiple parallel sensors satisfying the same function, is commonly used in industry. For example, commercial aircraft are equipped with triple or quadruple hardware redundancy for safety. This method is easy to implement and manage, however, there are also limitations. For instance, if one of the sensors is faulty, leaving only two sensors, it becomes more difficult to detect the failure because it cannot determine which of the remaining two sensors is healthy. The analytical redundancy method based on a mathematical model solves this limitation of hardware redundancy. Additionally, the analytical redundancy method has the advantage of reducing the cost and weight. This is useful for small UAVs with a limited payload.

The analytical redundancy method is divided into model-based and knowledge-based approaches. Model-based one uses a mathematical model. Knowledge-based one uses data collected through online monitoring according to a set of rules learned from human experts and past experiences [5]. As a model-based method, a filter-based method is widely used. There are studies that have performed sensor fault diagnosis using filter-based methods, such as KF, EKF [6, 7], and UKF [8]. Furthermore, a robust fault diagnosis method against model uncertainties is based on the EKF algorithm [9, 10]. Inspired by [7], this paper proposed a fault detection and diagnosis (FDD) scheme for the inertial measurement unit (IMU) sensor and actuators of a hexacopter UAV. We design the fault detection and isolation (FDI) algorithm using the analytical redundancy of angular rates. The fault detection of

gyroscope, accelerometer, and actuator is performed using dual EKF, each designed for the dynamics and kinematics of angular rates. Unlike [7] considering a satellite system, this paper considers a multicopter UAV. Moreover, our method can detect the partial fault of IMU as well as a complete fault on all axis. This fault diagnosis algorithm is tested through numerical simulations against bias sensor fault.

This paper is organized as follows. The hexacopter UAV modeling will be discussed in Section 2. In Section 3, the EKFs for fault diagnosis are designed. Then, Section 4 implements numerical simulations to confirm the fault detection performance. Finally, Section 5 summarizes the work of this paper.

2. Hexacopter UAV Modeling for Attitude Control

The configuration and coordinate system are shown in Fig. 1. The NED (North, East, Down) frame is used in this paper.

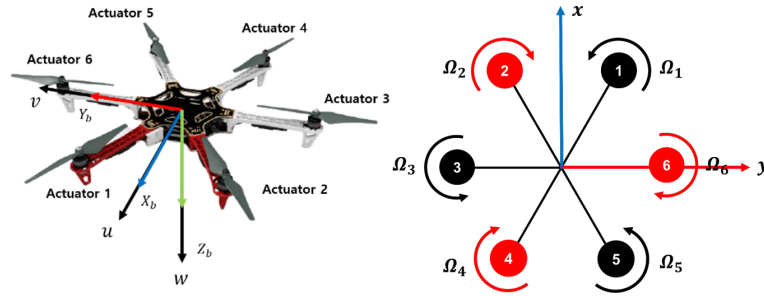


Figure 1 – The configuration of the hexacopter UAV

The attitude control system for a hexacopter UAV is represented in Fig. 2. The accelerometer and gyroscope are the measurement sensors for attitude estimation. The altitude control is additionally included for hover flight as shown in Fig. 2.

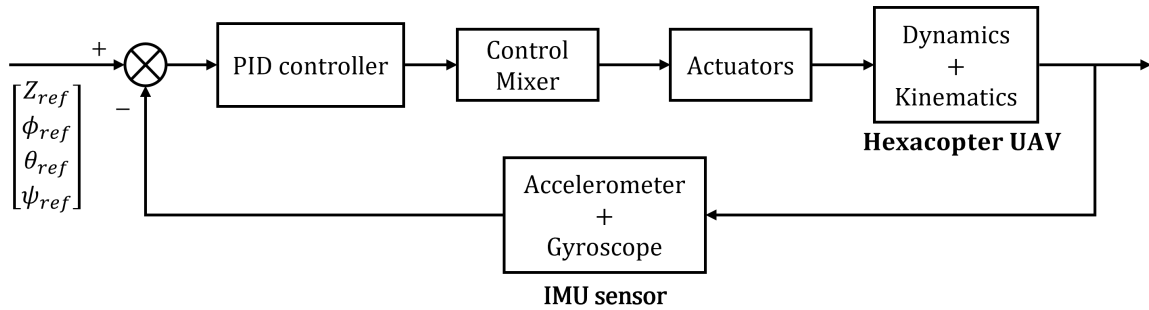


Figure 2 – A block diagram of the hexacopter UAV attitude control system

2.1 Dynamics Model

The dynamics model for a hexacopter UAV can be described as follows.

$$\dot{\omega} = I^{-1} \{ (M_c + M_{gyro}) - \omega \times (I\omega) \} \quad (1)$$

where $\omega = [p \ q \ r]^T$ is the angular rate vector, I is a moment of inertia matrix, and $M_c = [M_{c\phi}, M_{c\theta}, M_{c\psi}]^T$ & M_{gyro} denote a control torque and a gyroscopic moment. Expanding this element-wise gives

$$\begin{bmatrix} \dot{p} \\ \dot{q} \\ \dot{r} \end{bmatrix} = \begin{bmatrix} \left(\frac{I_{yy} - I_{zz}}{I_{xx}} \right) qr + \frac{q}{I_{xx}} I_{rzz} \Omega_{\Gamma} + \frac{1}{I_{xx}} M_{c\phi} \\ \left(\frac{I_{zz} - I_{xx}}{I_{yy}} \right) pr - \frac{p}{I_{yy}} I_{rzz} \Omega_{\Gamma} + \frac{1}{I_{yy}} M_{c\theta} \\ \left(\frac{I_{xx} - I_{yy}}{I_{zz}} \right) pq + \frac{1}{I_{zz}} M_{c\psi} \end{bmatrix} \quad (2)$$

where

$$\begin{aligned} M_{c_\phi} &= d_1 C_T (-\Omega_1^2 + \Omega_2^2 + \Omega_4^2 - \Omega_5^2) + d C_T (\Omega_3^2 - \Omega_6^2) \\ M_{c_\theta} &= d_2 C_T (\Omega_1^2 + \Omega_2^2 - \Omega_4^2 - \Omega_5^2) \\ M_{c_\psi} &= C_Q (\Omega_1^2 - \Omega_2^2 + \Omega_3^2 - \Omega_4^2 + \Omega_5^2 - \Omega_6^2) \end{aligned} \quad (3)$$

and

$$\Omega_\Gamma = \Omega_1 - \Omega_2 + \Omega_3 - \Omega_4 + \Omega_5 - \Omega_6 . \quad (4)$$

where $[\Omega_1, \Omega_2, \dots, \Omega_6]$ denotes the rotational speed of each propeller, d is the motor arm length, $d_1 = d \cos 60^\circ$, and $d_2 = d \sin 60^\circ$.

2.2 Kinematics Model

The kinematics model for the hexacopter UAV represents the rotational transformation between the body-axis angular rates and the Euler rates as follows [11].

$$\begin{bmatrix} \dot{\phi} \\ \dot{\theta} \\ \dot{\psi} \end{bmatrix} = \begin{bmatrix} p + q \sin \phi \tan \theta + r \cos \phi \tan \theta \\ q \cos \phi - r \sin \phi \\ q \sin \phi \sec \theta + r \cos \phi \sec \theta \end{bmatrix} \quad (5)$$

where $[p, q, r]^T$ is the body-axis angular rates, and $[\dot{\phi}, \dot{\theta}, \dot{\psi}]^T$ is the Euler rates.

3. Fault Diagnosis System based on Extended Kalman Filter

This section presents a fault diagnosis algorithm for the hexacopter attitude control system based on EKF. Figure 3 demonstrates the architecture of the fault detection considered in this paper.

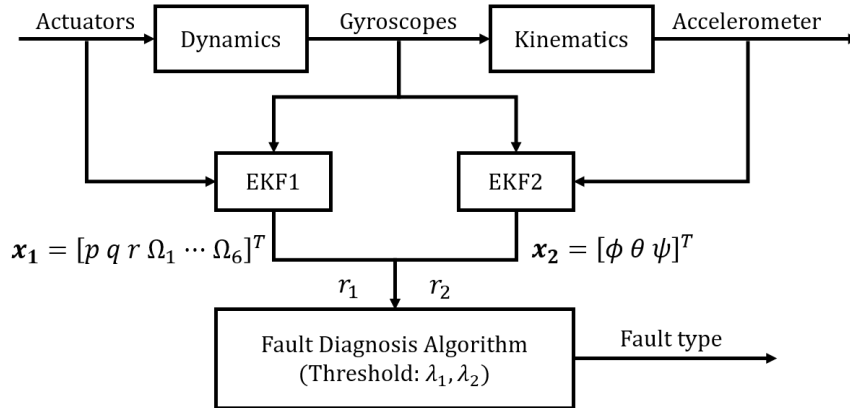


Figure 3 – The architecture of the fault diagnosis system

We design two EKFs to diagnose the system faults using the redundant relationship between the kinematics and dynamics models. The EKF1 designed based on the dynamics in Eq. 1 can detect a fault of actuators and the gyroscope. The other EKF2 designed based on the kinematics in Eq. 5 can detect a fault of the accelerometer and gyroscope. Because the gyroscope is the redundant component appeared in both kinematics and dynamics models, the fault diagnosis system of the gyroscope, accelerometer, and actuator can be designed by using the two EKFs and the redundant relationship of the hexacopter system.

3.1 Design of EKF-based on Dynamics

The state variable of the EKF1 is:

$$x_1 = [p \ q \ r \ \Omega_1 \ \Omega_2 \ \Omega_3 \ \Omega_4 \ \Omega_5 \ \Omega_6]^T . \quad (6)$$

The system equation about the state variable is defined as follows.

$$\dot{x}_1 = f_1(x_1, u) + \eta_1 \quad (7)$$

where x_1 is the state variable of the EKF1, u is the control input of the hexacopter system, that is angular rate vector of the six rotors (Ω_c). Element-wise representation is given as

$$\begin{bmatrix} \dot{p} \\ \dot{q} \\ \dot{r} \\ \dot{\Omega}_1 \\ \vdots \\ \dot{\Omega}_6 \end{bmatrix} = \begin{bmatrix} \left(\frac{I_{yy}-I_{zz}}{I_{xx}}\right)qr + \frac{q}{I_{xx}}I_{rzz}\Omega_\Gamma + \frac{1}{I_{xx}}M_{c\phi} \\ \left(\frac{I_{zz}-I_{xx}}{I_{yy}}\right)pr - \frac{p}{I_{yy}}I_{rzz}\Omega_\Gamma + \frac{1}{I_{yy}}M_{c\theta} \\ \left(\frac{I_{xx}-I_{yy}}{I_{zz}}\right)pq + \frac{1}{I_{zz}}M_{c\psi} \\ -\frac{1}{\tau_\Omega}(\Omega_1 - \Omega_{1c}) \\ \vdots \\ -\frac{1}{\tau_\Omega}(\Omega_6 - \Omega_{6c}) \end{bmatrix} + \begin{bmatrix} \eta_p \\ \eta_q \\ \eta_r \\ \eta_{\Omega_1} \\ \vdots \\ \eta_{\Omega_6} \end{bmatrix} \quad (8)$$

where τ_Ω is the rotor time constant, and Ω_{i_c} is the control command of the rotors.

The measurements of the EKF1 are the three-axis angular rates and z-axis acceleration that can be calculated by the angular rates of the six rotors [12]. The measurement equation is represented as follows:

$$y_1 = h_1(x_1) + v_1 + f_1 \quad (9)$$

$$\begin{bmatrix} p_m \\ q_m \\ r_m \\ a_z \end{bmatrix} = \begin{bmatrix} p \\ q \\ r \\ \sum_{i=1}^6 \frac{C_T \Omega_i^2}{m} \end{bmatrix} + \begin{bmatrix} v_g^p \\ v_g^q \\ v_g^r \\ v_A \end{bmatrix} + \begin{bmatrix} f_g^p \\ f_g^q \\ f_g^r \\ f_A \end{bmatrix} \quad (10)$$

where v_g & f_g are the measurement noise and the fault of the gyroscope, and v_A & f_A are the measurement noise and the fault of the actuators.

The above state and measurement equations of the EKF1 are discretized to the first order as follows:

$$\begin{aligned} x_{1k+1} &= f_1(x_{1k}, u_k) + w_{1k} \\ y_{1k} &= h_1(x_{1k}) + v_{1k} \end{aligned} \quad (11)$$

where w_{1k} is the system noise, and v_{1k} is the measurement noise. The Kalman filter has an algorithm that repeats the prediction and correction steps. In the prediction step, the predicted state is obtained using the system dynamics. In the correction step, the estimated state is obtained by correcting the predicted state using the measurement. The detailed equations of the prediction and correction steps are represented as follows.

Time update (Prediction)

$$\hat{x}_{1k}^- = f_1(\hat{x}_{1k-1}, u_{k-1}) \quad (12)$$

$$F_1 = \frac{\partial f_1}{\partial x_1} \Big|_{x_1 = \hat{x}_{1k-1}} \quad (13)$$

$$P_{1k}^- = F_1 P_{1k-1} F_1^T + Q_1 \quad (14)$$

Measurement update (Correction)

$$H_1 = \frac{\partial h_1}{\partial x_1} \Big|_{x_1 = \hat{x}_{1k}^-} \quad (15)$$

$$K_{1k} = P_{1k}^- H_1^T (H_1 P_{1k}^- H_1^T + R_1)^{-1} \quad (16)$$

$$\hat{x}_{1k} = \hat{x}_{1k}^- + K_{1k} \{y_{1k} - h_1(\hat{x}_{1k}^-)\} \quad (17)$$

$$P_{1k} = (I - K_{1k} H_1) P_{1k}^- \quad (18)$$

where \hat{x}_{1k}^- and \hat{x}_{1k} mean a priori and a posteriori estimates, respectively. F_1 and H_1 are the jacobian matrix of the nonlinear system and nonlinear measurement equation, respectively. $Q_1 \in \mathbb{R}^{9 \times 9}$ is the system noise covariance matrix. $R_1 \in \mathbb{R}^{4 \times 4}$ is the measurement noise covariance matrix.

3.2 Design of EKF-based on Kinematics

The state variable of the EKF2 is the Euler angles $x_2 = [\phi \ \theta \ \psi]^T$. The system equation for the EKF2 is defined as:

$$\dot{x}_2 = f_2(x_2) + \eta_2 \quad (19)$$

$$\begin{bmatrix} \dot{\phi} \\ \dot{\theta} \\ \dot{\psi} \end{bmatrix} = \begin{bmatrix} p + q \sin \phi \tan \theta + r \cos \phi \tan \theta \\ q \cos \phi - r \sin \phi \\ q \sin \phi \sec \theta + r \cos \phi \sec \theta \end{bmatrix} + \begin{bmatrix} \eta_\phi \\ \eta_\theta \\ \eta_\psi \end{bmatrix} \quad (20)$$

where $[p \ q \ r]^T$ is the known values measured by the gyroscope.

The measurements of the EKF2 are roll and pitch angles calculated by accelerometer measurements.

$$y_2 = H_2 x_2 + v_2 + f_2 \quad (21)$$

$$\begin{bmatrix} \phi_m \\ \theta_m \end{bmatrix} = \begin{bmatrix} 1 & 0 & 0 \\ 0 & 1 & 0 \end{bmatrix} \begin{bmatrix} \phi \\ \theta \\ \psi \end{bmatrix} + \begin{bmatrix} v_a^\phi \\ v_a^\theta \end{bmatrix} + \begin{bmatrix} f_a^\phi \\ f_a^\theta \end{bmatrix} \quad (22)$$

where v_a & f_a are the measurement noise and the fault of the accelerometer. The roll and pitch angle measurements are calculated by three-axis accelerations as Eq. 23 [13].

$$\phi_m = \tan^{-1} \left(\frac{a_y}{a_z} \right), \quad \theta_m = \tan^{-1} \left(\frac{a_x}{\sqrt{a_y^2 + a_z^2}} \right) \quad (23)$$

The above state and measurement equations of the EKF2 are discretized to the first order as follows:

$$\begin{aligned} x_{2_{k+1}} &= f_2(x_{2_k}) + w_{2_k} \\ y_{2_k} &= H_2 x_{2_k} + v_{2_k} \end{aligned} \quad (24)$$

where w_{2_k} is the system noise vector, and v_{2_k} is the measurement noise vector. The Kalman filter algorithm is the same as the EKF1. However, the measurement equation in the EKF2 is a linear equation, unlike the EKF1 measurement equation. The detailed equations of the EKF2 are represented as follows.

Time update (Prediction)

$$\hat{x}_{2_k}^- = f_2(\hat{x}_{2_{k-1}}) \quad (25)$$

$$F_2 = \left. \frac{\partial f_2}{\partial x_2} \right|_{x_2 = \hat{x}_{2_{k-1}}} \quad (26)$$

$$P_{2_k}^- = F_2 P_{2_{k-1}} F_2^T + Q_2 \quad (27)$$

Measurement update (Correction)

$$K_{2_k} = P_{2_k}^- H_2^T (H_2 P_{2_k}^- H_2^T + R_2)^{-1} \quad (28)$$

$$\hat{x}_{2_k} = \hat{x}_{2_k}^- + K_{2_k} (y_{2_k} - H_2 \hat{x}_{2_k}^-) \quad (29)$$

$$P_{2_k} = (I - K_{2_k} H_2) P_{2_k}^- \quad (30)$$

where $\hat{x}_{2_k}^-$ and \hat{x}_{2_k} mean a priori and a posteriori estimates, respectively. F_2 is the jacobian matrix of the nonlinear system equation. $Q_2 \in \mathbb{R}^{3 \times 3}$ and $R_2 \in \mathbb{R}^{2 \times 2}$ denote the system noise and the measurement noise covariance matrices, respectively.

3.3 Fault Diagnosis Algorithm

The fault diagnosis algorithm is designed based on the EKFs derived in the previous section. Fault diagnosis using the EKFs can detect a fault when the residual exceeds a specific threshold (λ). Here, the residual means the difference between the measurement and the predicted measurement. The residuals of the EKF1 and the EKF2 are shown as

$$\begin{aligned} r_1 &= y_1 - h_1(\hat{x}_1^-) \\ r_2 &= y_2 - H_2\hat{x}_2^- \end{aligned} \quad (31)$$

where $r_1 = [r_1^p \ r_1^q \ r_1^r \ r_1^{a_z}]^T$ and $r_2 = [r_2^\phi \ r_2^\theta]^T$ are the residuals generated by the EKFs based on dynamics and kinematics, respectively. Fault detection is performed using the RMS error of the residual as represented in Eq. 32. We assume that only one component among the accelerometer, actuator, or gyroscope can be faulty at a time.

$$\begin{cases} \|r(t)\|_{RMS} < \lambda, & \text{fault-free} \\ \|r(t)\|_{RMS} \geq \lambda, & \text{faulty} \end{cases} \quad (32)$$

3.3.1 Complete Fault Diagnosis

In this paper, a complete fault of the sensor means failure on all axes, and a complete fault of the actuator means that the actuator is turned off. Table 1 shows the algorithm for a complete fault of the gyroscope, accelerometer, and actuator. Since the accelerometer measurements are used in the z-axis acceleration of EKF1 and EKF2, if $r_1^{a_z}$ and r_2 exceed the thresholds, it is determined as an accelerometer fault. A gyroscope fault is detected when all residuals excluding the z-axis acceleration of EKF1 exceed the threshold. This is because the gyroscope measurements are used in the angular-rates dynamics of EKF1 and kinematics of EKF2. Also, the z-axis acceleration of EKF1 is measured from the accelerometer. The angular velocities of the actuator are used only in EKF1. However, in the physical aspect, if a specific actuator fails, attitude changes are inevitable. Therefore, an actuator fault is detected when all residuals exceed the threshold.

Table 1 – Fault diagnosis algorithm for a complete fault ($r_1^{gyro} = [r_1^p \ r_1^q \ r_1^r]^T$ and $\lambda_1^{gyro} = [\lambda_1^p \ \lambda_1^q \ \lambda_1^r]^T$)

No.	Diagnostic logic	Fault type
1	$\ r_1^{gyro}\ < \lambda_1^{gyro}, \ r_1^{a_z}\ < \lambda_1^{a_z} \ \& \ \ r_2\ < \lambda_2$	Fault-free
2	$\ r_1^{gyro}\ < \lambda_1^{gyro}, \ r_1^{a_z}\ \geq \lambda_1^{a_z} \ \& \ \ r_2\ \geq \lambda_2$	Accelerometer fault
3	$\ r_1^{gyro}\ \geq \lambda_1^{gyro}, \ r_1^{a_z}\ < \lambda_1^{a_z} \ \& \ \ r_2\ \geq \lambda_2$	Gyroscope fault
4	$\ r_1^{gyro}\ \geq \lambda_1^{gyro}, \ r_1^{a_z}\ \geq \lambda_1^{a_z} \ \& \ \ r_2\ \geq \lambda_2$	Actuator fault

3.3.2 Partial Fault Diagnosis

A partial fault is defined as the fault of only one axis of the three-axis accelerometer or gyroscope, and a partial fault of the actuator is not considered in this paper. Table 2 and 3 represent the fault detection algorithm of a partial fault for the accelerometer and gyroscope, respectively. For the partial fault of the accelerometer, the z-axis fault is not considered. In general, the z-axis measurement is dominant in the accelerometer measurement. Thus, a fault in the z-axis can be regarded as a complete fault.

Table 2 – Fault diagnosis algorithm for a partial fault of accelerometer

No.	Diagnostic logic	Fault type
21	$\ r_1\ < \lambda_1 \ \& \ \ r_2^\phi\ < \lambda_2^\phi, \ r_2^\theta\ \geq \lambda_2^\theta$	x-axis fault
22	$\ r_1\ < \lambda_1 \ \& \ \ r_2^\phi\ \geq \lambda_2^\phi, \ r_2^\theta\ < \lambda_2^\theta$	y-axis fault

Table 3 – Fault diagnosis algorithm for a partial fault of gyroscope

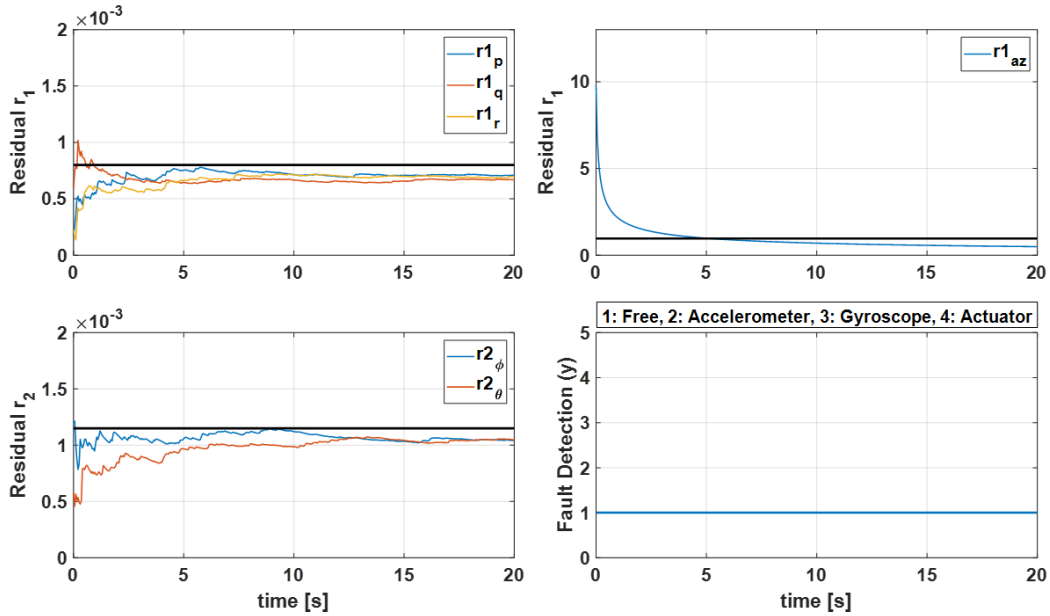
No.	Diagnostic logic	Fault type
31	$\ r_1^p\ \geq \lambda_1^p, \ r_1^q\ < \lambda_1^q, \ r_1^r\ < \lambda_1^r, \ r_1^{a_z}\ < \lambda_1^{a_z}$ & $\ r_2^\phi\ \geq \lambda_2^\phi, \ r_2^\theta\ < \lambda_2^\theta$	x-axis fault
32	$\ r_1^p\ < \lambda_1^p, \ r_1^q\ \geq \lambda_1^q, \ r_1^r\ < \lambda_1^r, \ r_1^{a_z}\ < \lambda_1^{a_z}$ & $\ r_2^\phi\ < \lambda_2^\phi, \ r_2^\theta\ \geq \lambda_2^\theta$	y-axis fault
33	$\ r_1^p\ < \lambda_1^p, \ r_1^q\ < \lambda_1^q, \ r_1^r\ \geq \lambda_1^r, \ r_1^{a_z}\ < \lambda_1^{a_z}$ & $\ r_2^\phi\ < \lambda_2^\phi, \ r_2^\theta\ < \lambda_2^\theta$	z-axis fault

4. Numerical Simulation

In this section, numerical simulations are conducted to verify the performance of the fault diagnosis algorithm. We select maintaining a hovering flight at an altitude of 5 m as a fault-free case. The thresholds of the EKF1 and EKF2 are determined by fault-free case simulations shown in Fig. 4. Since the difference between the residuals of the angular rates and the z-axis acceleration is large, the threshold of EKF1 is divided into two as in Eq. 33. As shown in Fig. 4, all the residuals of the EKF1 and the EKF2 are smaller than the thresholds in a fault-free case.

$$\lambda_1 = \begin{cases} 8 \times 10^{-4} & \text{for angular rates } (\lambda_1^{gyro}) \\ 0.96 & \text{for z-axis acceleration } (\lambda_1^{a_z}) \end{cases} \quad (33)$$

$$\lambda_2 = 1.15 \times 10^{-3}$$


 Figure 4 – Fault diagnosis simulation results - Fault-free ($y = 1$)

4.1 Complete Fault

Following the fault-free case, the sensor fault simulations are conducted by applying a bias fault to the accelerometer (f_a) and the gyroscope (f_g). The actuator fault simulation is performed by causing actuator 3 of the hexacopter shown in Fig. 1 to turn off at 5 seconds. The bias faults of the accelerometer and gyroscope are described in Eq. 34 and 35, respectively.

$$f_a = \begin{cases} 0 & t < 5s \\ 5m/s^2 & t \geq 5s \end{cases} \quad (34)$$

$$f_g = \begin{cases} 0 & t < 5s \\ 5deg/s & t \geq 5s \end{cases} \quad (35)$$

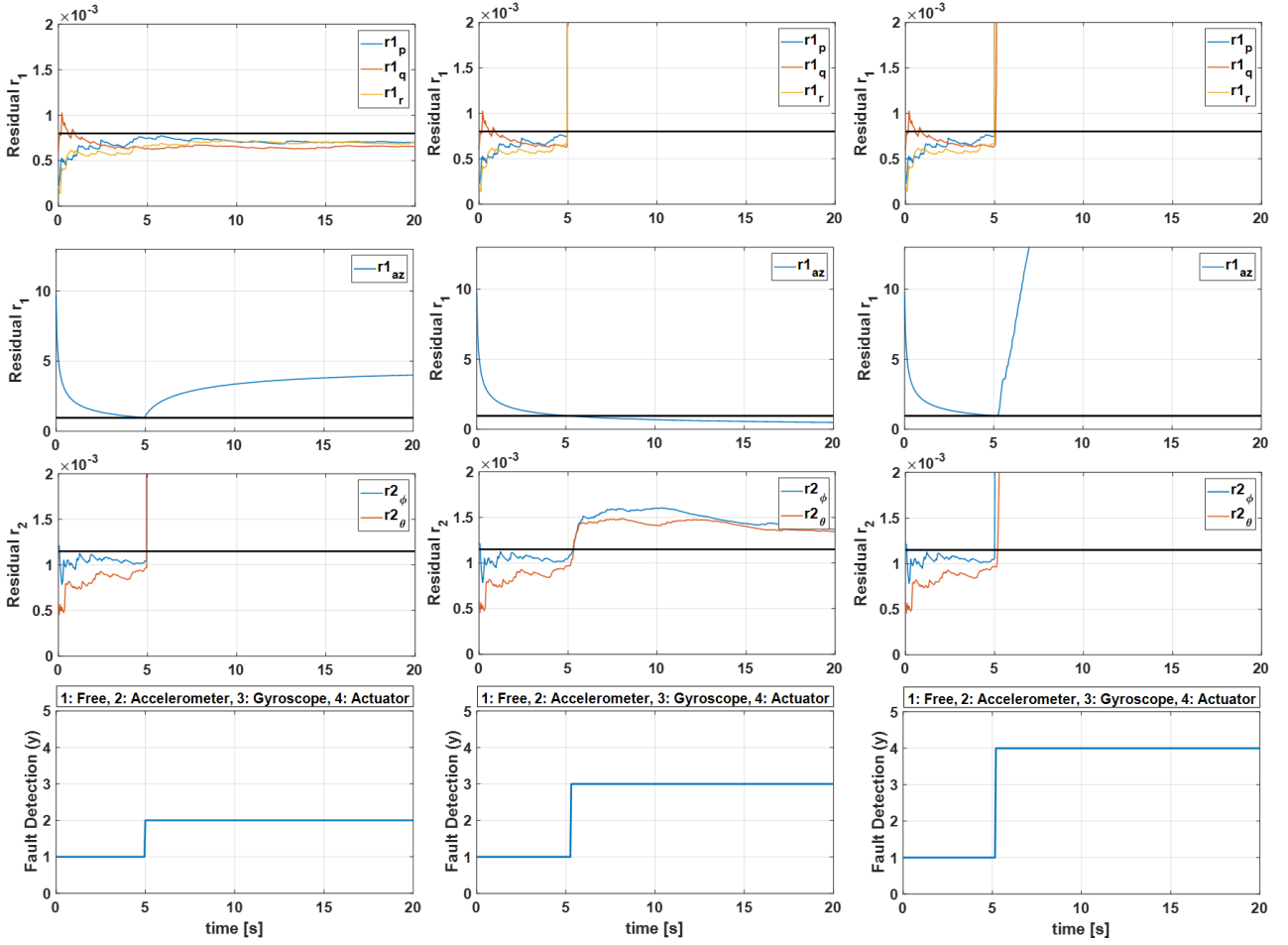


Figure 5 – Fault diagnosis simulation results - Complete fault ($y = 2$: accelerometer, $y = 3$: gyroscope, and $y = 4$: actuator)

Figure 5 shows the simulation results of the accelerometer, gyroscope, and actuator in order. The results on the left side of Fig. 5 demonstrate that the fault detection module detects the accelerometer fault when $r_1^{a_z}$ and r_2 exceed the thresholds. Since the z-axis acceleration of EKF1 is measured from the accelerometer, and the accelerometer measurements are used to estimate the attitude angle in EKF2, it can be seen that $r_1^{a_z}$ and r_2 exceed the thresholds. The gyroscope measurements are used in both dynamics(EKF1) and kinematics(EKF2) of angular rates. Thus, the gyroscope fault is detected when $r_1^{s_{yro}}$ and r_2 exceed the thresholds at the same time. Note that $r_1^{a_z}$ does not exceed the threshold as the gyroscope is independent of the actuator dynamics of EKF1. Also, there is a time delay of about 0.3 seconds to detect the gyroscope fault. This time delay occurs because the attitude angle estimated by the EKF2 is calculated from the accelerometer measurements rather than directly using the gyroscope measurements. Finally, the results on the right side of Fig. 5 show that actuator fault is detected when all residuals exceed the thresholds. This is because, as mentioned in the previous section, the actuator fault induces an immediate attitude change. There is a time delay of about 0.2 seconds to detect the actuator fault. This time delay is an acceptable range, but it can be reduced by adjusting the threshold $\lambda_1^{a_z}$. Although not shown in this paper, the same fault detection performance is shown in other actuator failures.

4.2 Partial Fault

Same as the complete fault, the simulations of a partial fault are performed by injecting the bias into each axis of the sensors. Figure 6 represents the fault detection results for each axis of the accelerometer. Since the x-axis translation leads to a change in pitch angle(θ), the fault of the x-axis accelerometer is detected when r_2^θ exceeds λ_2^θ . Similarly, the y-axis translation leads to roll angle(ϕ) change, the fault of the y-axis accelerometer is detected when r_2^ϕ exceeds λ_2^ϕ .

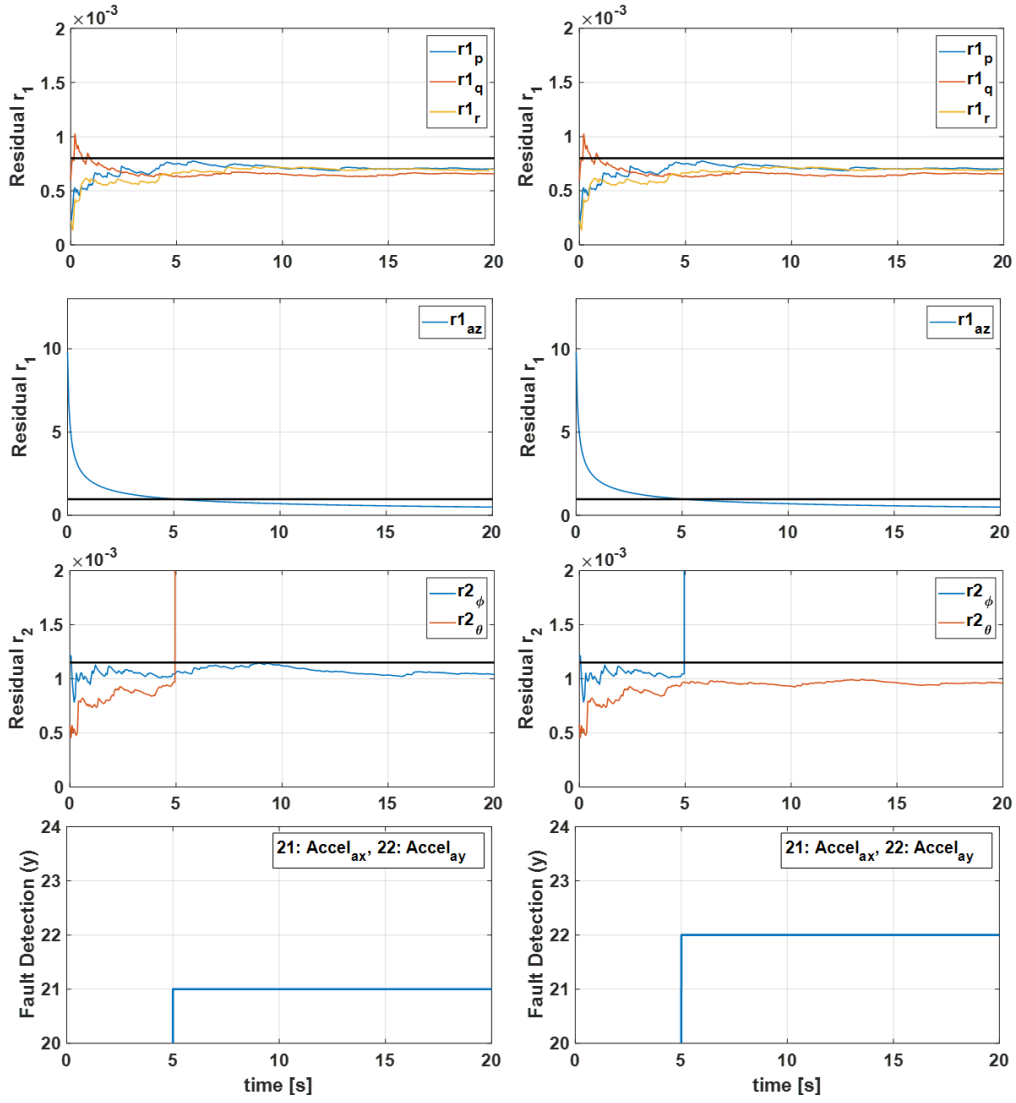


Figure 6 – Fault diagnosis simulation results - Partial fault of accelerometer
($y = 21$: x-axis and $y = 22$: y-axis)

Figure 7 gives the x-, y-, and z-axis fault detection results of the gyroscope in order. The x-, y-, and z-axis gyroscopes measure p , q , and r , respectively. In hover flight conditions, p measurement error affects roll angle (ϕ), and q measurement error affects theta angle (θ) due to the kinematics of angular rates. Therefore, the x-axis fault is detected when r_1^p and r_2^ϕ exceed thresholds, and the y-axis fault is detected when r_1^q and r_2^θ exceed thresholds. Since the yaw angle (ψ) is not used as the measurement of the EKF2, z-axis fault is detected when only r_1^r exceeds the threshold λ_1^r .

5. Conclusion

This paper conducted fault diagnosis for a hexacopter UAV attitude control system. We designed two extended Kalman filters based on the dynamics and kinematics of the vehicle. Using these estimators, the fault detection of the gyroscope, the accelerometer, and the actuator was successfully conducted. Moreover, it was verified through the simulations that both complete and partial fault of the sensors was possible to detect. However, for the fault of the IMU sensor (gyroscopes + accelerometers), there are various fault situations such as drift, loss of accuracy, loss of effectiveness, as well as bias fault. In addition, for the fault of the actuator, it is not enough to simply detect whether the actuator has failed since a multicopter has multiple actuators. To cope with the detected fault, it is necessary to diagnose which actuator is a failure. Therefore, more detailed fault detection in various fault situations will be conducted in the future.

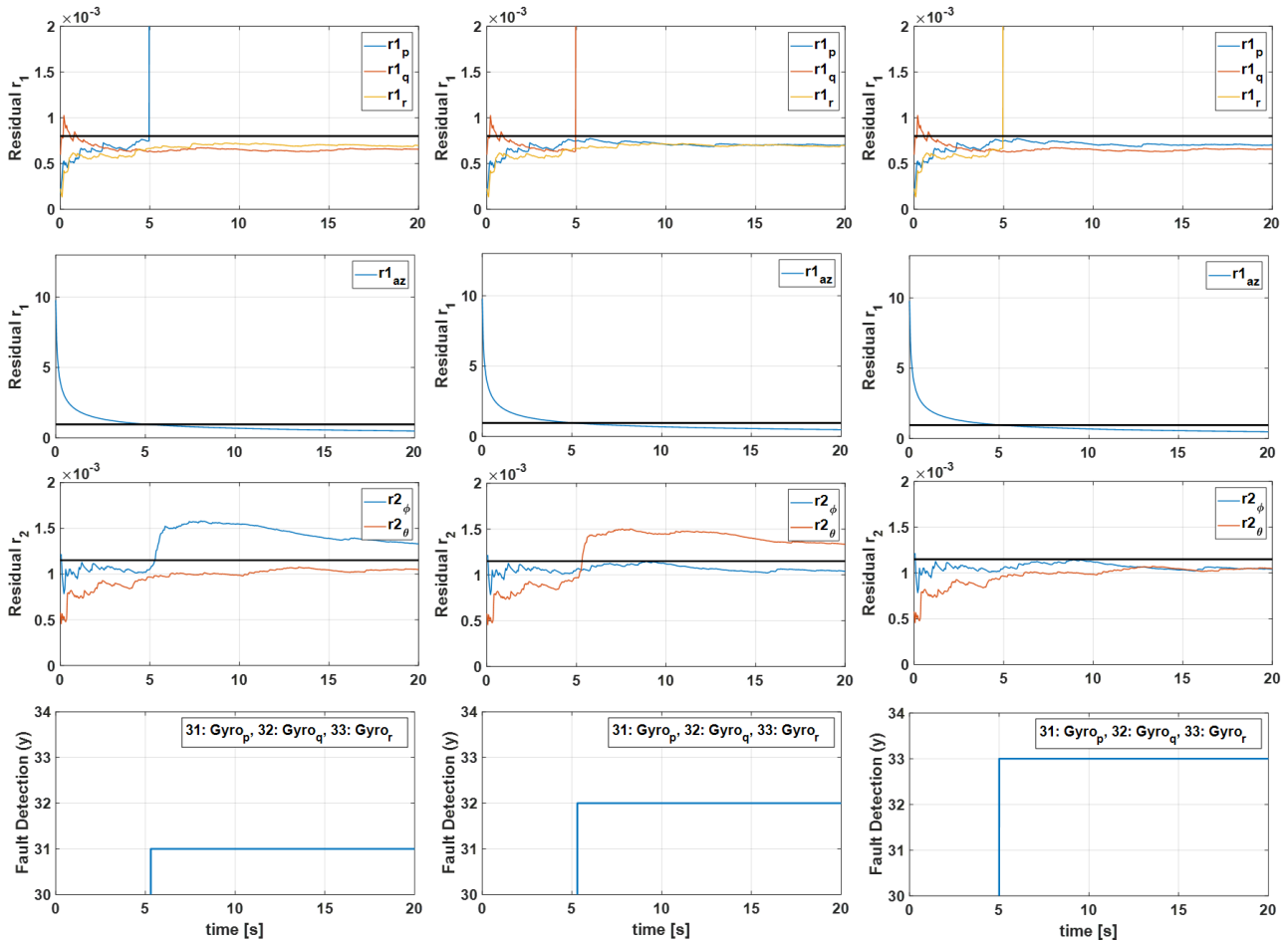


Figure 7 – Fault diagnosis simulation results - Partial fault of gyroscope
 ($y = 31$: x-axis, $y = 32$: y-axis, and $y = 33$: z-axis)

6. Contact Author Email Address

mailto: skim78@cnu.ac.kr (corresponding author)
 mailto: yjk980702@g.cnu.ac.kr

7. Copyright Statement

The authors confirm that they, and/or their company or organization, hold copyright on all of the original material included in this paper. The authors also confirm that they have obtained permission, from the copyright holder of any third party material included in this paper, to publish it as part of their paper. The authors confirm that they give permission, or have obtained permission from the copyright holder of this paper, for the publication and distribution of this paper as part of the ICAS proceedings or as individual off-prints from the proceedings.

Acknowledgment

This research was supported by Unmanned Vehicles Core Technology Research and Development Program through the National Research Foundation of Korea (NRF) and Unmanned Vehicle Advanced Research Center (UVARC) funded by the Ministry of Science and ICT, the Republic of Korea (2020M3C1C1A01083162)

References

- [1] H. Shakhathreh, A. Sawalmeh, A. Al-Fuqaha, Z. Dou, E. Almaita, I. Khalil, N. Othman, A. Khreishah, and M. Guizani. Unmanned aerial vehicles: A survey on civil applications and key research challenges. *IEEE Access*, Vol. 7, pp 48572-48634, 2019.
- [2] Lieret, M., Fertsch, J. and Franke, J. Fault detection for autonomous multirotors using a redundant flight control architecture. *2020 IEEE 16th International Conference on Automation Science and Engineering (CASE)*, pp 29-34, 2020.

- [3] Lu, P. Fault diagnosis and fault-tolerant control for aircraft subjected to sensor and actuator faults. 2016.
- [4] Fourlas, George K., and George C. Karras. A survey on fault diagnosis methods for UAVs. *2021 International Conference on Unmanned Aircraft Systems (ICUAS)*, pp 394-403, 2021.
- [5] Nan, C., Khan, F., and Iqbal, M. T. Real-time fault diagnosis using knowledge-based expert system. *Process safety and environmental protection*, Vol. 86, No. 1, pp 55-71, 2008.
- [6] Jayaram, S. A new fast converging Kalman filter for sensor fault detection and isolation. *Sensor Review*, 2010.
- [7] Gao, S., Zhang, Z., Zhang, W., He, X., and Lu, X. Fault diagnosis for satellite attitude control system with using extended Kalman filter. *In 2019 Chinese Control Conference (CCC)*, pp 4789-4794, 2019.
- [8] Bae, J. H., and Kim, Y. D. Attitude estimation for satellite fault tolerant system using federated unscented Kalman filter. *International Journal of Aeronautical and Space Sciences*, Vol. 11, 2, pp 80-86, 2010.
- [9] Lu, P., Van Eykeren, L., Van Kampen, E. J., Chu, Q. P., and Yu, B. Adaptive hybrid unscented Kalman filter for aircraft sensor fault detection, isolation and reconstruction. *In AIAA guidance, navigation, and control conference*, pp 1145, 2014.
- [10] Zhong, Y., Zhang, W., Zhang, Y., Zuo, J., and Zhan, H. Sensor fault detection and diagnosis for an unmanned quadrotor helicopter. *Journal of Intelligent & Robotic Systems*, Vol. 96, No. 3, pp 555-572, 2019.
- [11] Stevens, B. L., Lewis, F. L., and Johnson, E. N. *Aircraft control and simulation: dynamics, controls design, and autonomous systems*. 3rd edition, John Wiley & Sons, 2015.
- [12] Kim. T. and Kim. S. Actuator Fault Diagnosis and Counterplan Using Extended Kalman Filter Considering Symmetry of Hexacopter UAV. *Journal of Institute of Control, Robotics and Systems*, Vol. 27, No. 7, pp 473-481, 2021.
- [13] Leishman, R. C., Macdonald, J. C., Beard, R. W., and McLain, T. W. Quadrotors and accelerometers: State estimation with an improved dynamic model. *IEEE Control Systems Magazine*, Vol. 34, No. 1, pp 28-41, 2014.